Analysis of PIV interrogation for inhomogeneous image fields

by

J. Westerweel

Laboratory for Aero and Hydrodynamics
Delft University of Technology
Mekelweg 2, 2628 CD Delft, The Netherlands

ABSTRACT

The bias error in the PIV interrogation result is evaluated for the case of inhomogeneous images. An approximate expression is derived, by means of a perturbation analysis, which relates the bias error to the displacement, source density and image inhomogeneity. Three cases are investigated: (1) a gradient in the illumination; (2) a light-sheet with a thin shadow; and (3) a gradient in the mean intensity that moves with the tracer pattern. It is found that the magnitude of the bias error is of the order of the random error amplitude. It can therefore be concluded that the PIV interrogation (for a uniform displacement field) is very robust with respect to local variations in the image statistical properties.

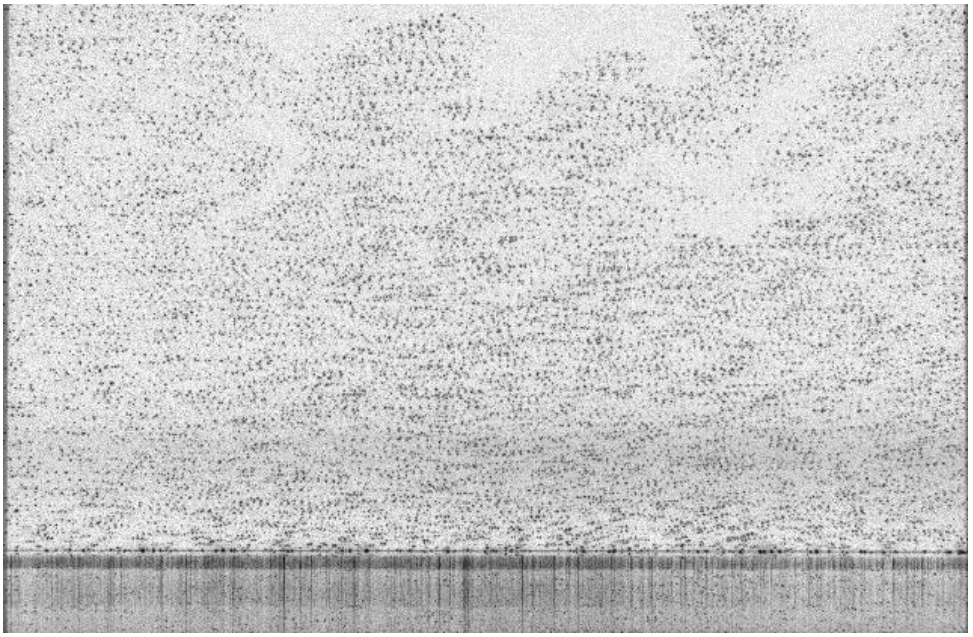

Figure 1 Image Im06 from the PivNet database (**http://pivnet.sm.go.dlr.de**) of a boundary layer flow. Note the inhomogeneous seeding in the outer flow region.

1. INTRODUCTION

The conventional theoretical analysis of PIV interrogation assumes a homogeneous distribution of tracer particles in the flow (Adrian 1988; Westerweel 1993). This condition implies that the spatial correlation yields a measurement of the displacement field that is not biased with respect to the spatial distribution of the particle images. To obtain a homogeneous image field it is necessary (1) to have ideal tracer particles that perfectly follow the motion of the fluid, and (2) to have an initial homogeneous distribution of tracer particles. It is also necessary that the mean size and intensity amplitude of the particle images is independent of the position within the image field.

These conditions are only met under ideal circumstances, which can only be approximated in practical situations; it is very common that there will be variations in the intensity profile of the laser light sheet, or that there is locally a higher concentration of tracer particles. An example of a PIV image with a small degree of inhomogeneity is shown in Figure 1. When such variations appear over a scale that is much larger than the size of the interrogation region, then the effects of the inhomegeneity are generally assumed to be negligible. For example, suppose that the light sheet intensity has a Gaussian intensity distribution in the direction parallel to the light sheet plane, so that particle images in the middle section of the image appear to be brighter than those near the edges. This typically occurs when a light sheet is formed by means of expanding a laser beam in one direction with a cylindrical lens. In these cases the length scale over which the intensity varies substantially is of the order of the image size, which is typically 30-100 times the diameter of the interrogation area.

The situation is quite different when there are sharp changes in the seeding density, or in the mean size of the particle images. This typically occurs for flows with inhomogeneous seeding. Non-ideal tracer particles with an initial homogeneous distribution over the flow at one given time instant, will eventually segregate, where the rate of segregation depends on the size and mass of the tracer particles. An example is a strong vortical flow, in which tracer particles with a specific gravity that is greater than that of the fluid is forced away from the vortex core. Another example is the lift force due to strong velocity gradients (e.g., in the near-wall region of a boundary layer flow) that acts on tracer particles with a finite diameter.

In other situations the tracer particles may not be well mixed with the fluid. This typically occurs when tracer particles are introduced into the flow at a single location somewhere upstream the measurement location; for flows with a low turbulence level there is no effective mixing mechanism that can distribute the tracer particles evenly over the fluid. Another common situation occurs when two flows merge, for example in a mixing layer, or in a jet. When the two flows are seeded at different concentrations, the image fields in the mixing region will be inhomogeneous.

2. HOMOGENEOUS IMAGE FIELDS

First the analysis of homogeneous image fields by Adrian (1988) and Keane & Adrian (1992) is reviewed.

Consider two image frames $I_1(\mathbf{X})$ and $I_2(\mathbf{X})$ that represent the pattern of tracer particles in the light sheet at times t_1 and t_2 respectively. The spatial correlation is given by:

$$R(\mathbf{s}) = \int W_1(\mathbf{X}) W_2(\mathbf{X}+\mathbf{s}) I_1(\mathbf{X}) I_2(\mathbf{X}+\mathbf{s}) d\mathbf{X} \tag{1}$$

where W_1 and W_2 represent the interrogation windows in I_1 and I_2 respectively.

Given that the tracers are distributed homogeneously over the flow, the mean image intensity is a constant. It is then convenient to separate the image fields into mean and fluctuating parts, i.e.

$$I_1(\mathbf{X}) = \langle I_1 \rangle + I_1'(\mathbf{X}) \quad \text{and} \quad I_2(\mathbf{X}) = \langle I_2 \rangle + I_2'(\mathbf{X}) \tag{2}$$

with: $\langle I_1'(\mathbf{X}) \rangle = \langle I_2'(\mathbf{X}) \rangle = 0$. The mean image intensities $\langle I_1 \rangle$ and $\langle I_2 \rangle$ are given by:

$$\langle I_1 \rangle = J_1 t_{00} C \Delta z_0 / M_0^2 \quad \text{and} \quad \langle I_2 \rangle = J_2 t_{00} C \Delta z_0 / M_0^2 \tag{3}$$

where J_1 and J_2 are the total light-sheet energies for I_1 and I_2 respectively, t_{00} is the total intensity for a single particle image (assuming that all tracer particles are identical), C the tracer number density, Δz_0 the light-sheet thickness, and M_0 the image magnification.

The conditional mean of $R(\mathbf{s})$ over the ensemble of all possible realizations of the pattern of tracer particles and for a given uniform velocity $\mathbf{u}$ is given by:

$$\langle R(\mathbf{s}) | \mathbf{u} \rangle = \langle R_C(\mathbf{s}) | \mathbf{u} \rangle + \langle R_D(\mathbf{s}) | \mathbf{u} \rangle + \langle R_F(\mathbf{s}) | \mathbf{u} \rangle \tag{4}$$

where the first term on the right represents the ensemble mean correlation of the mean image fields, and the second term on the right the ensemble mean correlation of the fluctuating image fields. The third term, representing the ensemble mean correlation of the mean and fluctuating image fields, is identical zero. The two remaining terms are given by:

$$\langle R_C(\mathbf{s})|\mathbf{u}\rangle = F_I(\mathbf{s})\langle I_1\rangle\langle I_2\rangle D_I^2$$
$$\langle R_D(\mathbf{s})|\mathbf{u}\rangle = J_1 J_2 t_{00}^2 N_I F_O(\Delta z) F_I(\mathbf{s}) F_t(\mathbf{s}-\mathbf{s}_D) \quad (5)$$

where F_I is defined as:

$$F_I(\mathbf{s}) = \frac{1}{D_I^2}\int W_1(\mathbf{X})W_2(\mathbf{X}+\mathbf{s})d\mathbf{X}, \quad (6)$$

D_I is the size of the interrogation region, N_I (= $(C\,\Delta z_0 / M_0^2)\,D_I^2$) the image density, F_O the loss-of-correlation due to the out-of-plane motion Δz, $F_t(\mathbf{s})$ the particle-image self-correlation, and $\mathbf{s}_D$ the in-plane particle-image displacement. For Gaussian particle images the particle-image self-correlation is given by:

$$F_t(\mathbf{s}) = \left(\frac{\pi}{4}d_t^2\right)\exp\left(-4s^2/d_t^2\right), \quad (7)$$

where d_t is the particle-image diameter.

For the present analysis of continuous image fields, the particle-image displacement is estimated by means of the centroid m_D of $R(\mathbf{s})$, i.e.

$$m_D = \frac{\int \mathbf{s}R(\mathbf{s})d\mathbf{s}}{\int R(\mathbf{s})d\mathbf{s}}. \quad (8)$$

In the case of discrete image fields the centroid estimate is known to be sensitive to the finite discretization of the image field (Prasad *et al*. 1992), and it is more common to use different estimators, such as *the three-point Gaussian fit* (Willert & Gharib 1991). The results for the centroid of the correlation peak should also hold for the three-point Gaussian fit provided that the effects of image discretization area negligible. In the case of diffraction-limited imaging the discretization matches the Nyquist sampling frequency when the particle-image diameter is at least four times the sample dimension, i.e. $d_t / d_r > 4$, and for the particle-image centroid bias errors due to finite discretization are negligible for $d_t / d_r > 2$ (Westerweel 1998). It is therefore assumed that the present analysis for the peak centroid also apply to other sub-pixel estimation methods.

The expectation of the centroid estimate is approximately given by (Adrian 1988):

$$\langle m_D|\mathbf{u}\rangle \cong \frac{\int \mathbf{s}\langle R(\mathbf{s})|\mathbf{u}\rangle d\mathbf{s}}{\int \langle R(\mathbf{s})|\mathbf{u}\rangle d\mathbf{s}} \quad (9)$$

(This expression would be exact when the numerator and denominator in (9) are statistically independent.) This completes the review of the work by Adrian (1988) and Keane & Adrian (1992), and below the ensemble-mean of the centroid is further investigated.

Substitution of (4) yields an expression for $\langle m_D|\mathbf{u}\rangle$. Please note that the term $\langle R_C(\mathbf{s})|\mathbf{u}\rangle$ in biases $\langle m_D|\mathbf{u}\rangle$. This term vanishes when the mean image intensity is subtracted from the image fields. Substitution of (5) yields:

$$\langle m_D|\mathbf{u}\rangle \cong \frac{\int \mathbf{s}F_I(\mathbf{s})F_t(\mathbf{s}-\mathbf{s}_D)d\mathbf{s}}{\int F_I(\mathbf{s})F_t(\mathbf{s}-\mathbf{s}_D)d\mathbf{s}} \quad (10)$$

In general the width of F_t is much smaller than the width of F_I, i.e. $d_t << D_I$. Hence, $F_I(\mathbf{s})$ is written as a Taylor series around $\mathbf{s}_D$:

$$F_I(\mathbf{s}) = F_I(\mathbf{s}_D) + (\mathbf{s}-\mathbf{s}_D)\left.\frac{\partial F_I(\mathbf{s})}{\partial \mathbf{s}}\right|_{\mathbf{s}=\mathbf{s}_D} + \text{h.o.} \quad (11)$$

Substitution in (10) yields

$$m_D \cong \mathbf{s}_D + \frac{1}{F_I(\mathbf{s}_D)}\left[\frac{\int \mathbf{s}F_t(\mathbf{s})d\mathbf{s}}{\int F_t(\mathbf{s})d\mathbf{s}}\left.\frac{\partial F_I(\mathbf{s})}{\partial \mathbf{s}}\right|_{\mathbf{s}=\mathbf{s}_D}\right] \quad (12)$$

where the term between brackets is the second moment of $F_t(\mathbf{s})$.

In general $\partial F_t(\mathbf{s})/\partial \mathbf{s}$ oriented towards the origin, i.e. $\mathbf{s} = \mathbf{0}$, and $F_I(\mathbf{s})$ and the second moment of $F_t(\mathbf{s})$ are both positive, so that m_D is usually biased towards a smaller absolute displacement. Below the results are given for Gaussian and uniform interrogation windows.

For identical Gaussian interrogation windows with a diameter D_I, $F_I(\mathbf{s})$ and its gradient are given by:

$$F_I(\mathbf{s}) = \exp\left(-8s^2/D_I^2\right), \text{ and: } \left.\frac{\partial F_I(\mathbf{s})}{\partial \mathbf{s}}\right|_{\mathbf{s}=\mathbf{s}_D} = -F_I(\mathbf{s}_D)\cdot 8\mathbf{s}_D/D_I^2, \quad (13)$$

respectively. The second moment of $F_t(\mathbf{s})$ for Gaussian particle images is $\frac{1}{8}d_t^2$, so the mean bias error $\mathbf{b}(\mathbf{s}_D) \equiv \langle m_D|\mathbf{u}\rangle - \mathbf{s}_D$ is given by:

$$\mathbf{b}(\mathbf{s}_D) \cong \mathbf{s}_D \frac{d_t^2}{D_I^2}, \tag{14}$$

i.e. the bias error is directly proportional to the displacement. This result is identical to the exact analytical result obtained by Keane & Adrian (1990).

For identical square uniform interrogation windows $F_I(\mathbf{s})$ is given by:

$$F_I(s,t) = \begin{cases} \left(1-|s|/D_I\right)\left(1-|t|/D_I\right) & |s|,|t| \le D_I \\ 0 & \text{elsewhere} \end{cases} \tag{15}$$

Consider only one component of $\mathbf{s}$; the spatial derivative of F_I with respect to s is given by:

$$\left.\frac{\partial F_I(\mathbf{s})}{\partial \mathbf{s}}\right|_{\mathbf{s}=\mathbf{s}_D} = -\frac{1}{D_I}\frac{s_D}{|s_D|}\frac{1}{1-|t_D|/D_I} \tag{16}$$

with: $\mathbf{s}_D = (s_D, t_D)$. (A similar expression can be found for the direction perpendicular to the direction of s.) The mean bias error is then given by:

$$b(s_D) = -\frac{1}{D_I}\frac{s_D}{|s_D|}\frac{1}{F_I(\mathbf{s}_D)}\frac{d_t^2}{8D_I^2}. \tag{17}$$

As second order and higher order derivatives of F_I are zero, this expression is exact.

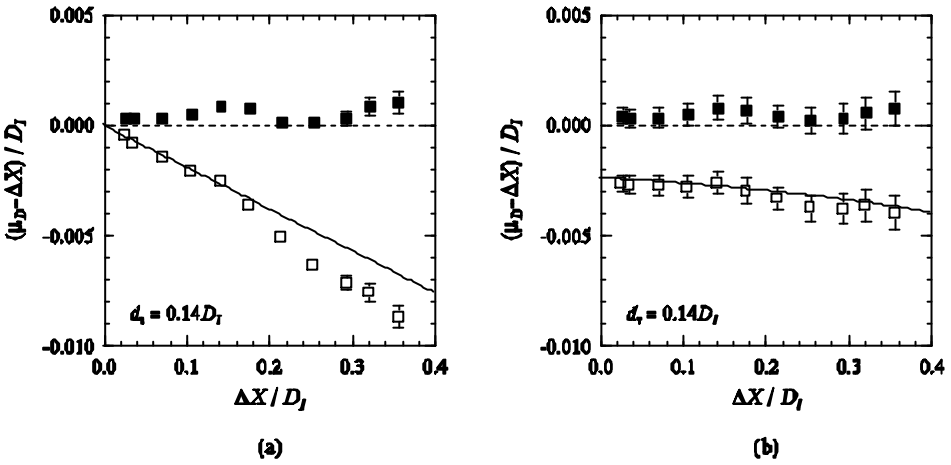

Figure 2 The displacement bias error as a function of the particle-image displacement for (a) Gaussian interrogation windows, and (b) uniform interrogation windows. Solid lines represent the analytical results in (14) and (17) respectively; the symbols are results obtained from uniformly translated test images (□ without bias correction; ■ with bias correction). From: Westerweel (1997).

In Figure 2 the results in (14) and (17) are compared against measurements of uniformly translated test images. The agreement between the results and actual measurements (open symbols) is quite good, in particular for small displacements, i.e. $|\Delta X|/D_I < 0.3$. In general this bias error can be avoided in two ways. The first one is to divide the spatial correlation by F_I, which can be determined by means of (6) (Westerweel 1997); the other way is to use uniform interrogation windows of different dimensions (Keane & Adrian 1992) such that F_I includes a region where it is constant, i.e. $\partial F_t(\mathbf{s})/\partial \mathbf{s} = \mathbf{0}$. The result for the bias correction by F_I-normalization is included in Figure 2 (closed symbols).

3. INHOMOGENEOUS IMAGE FIELDS

In this section the analysis of the bias error is carried out for the case of an inhomogeneous image field. In this case the mean image intensities $\langle I_1 \rangle$ and $\langle I_2 \rangle$ are functions of **X,** and the term $\langle R_C(\mathbf{s})|\mathbf{u}\rangle$ in (4) is given by:

$$\langle R_C(\mathbf{s})|\mathbf{u}\rangle = \int W_1(\mathbf{X})W_2(\mathbf{X}+\mathbf{s})\langle I_1(\mathbf{X})\rangle\langle I_2(\mathbf{X}+\mathbf{s})\rangle d\mathbf{X}. \tag{18}$$

For the present analysis the displacement field is considered to be uniform (i.e., the variation of the displacement field over the interrogation domain is negligible with respect to the of the displacement-correlation peak). So, the spatial variation of $C(\mathbf{X})$ does not affect the shape of the displacement-correlation peak. This is easily understood if one realizes that each particle-image pair contributes to $R_D(\mathbf{s})$ at the same location, i.e. only at $\mathbf{s} = \mathbf{s}_D$.

The aim of the present analysis is to determine the sensitivity of the PIV interrogation for inhomogeneous image fields. Rather than going through a rigorous generalization of the equations derived for the ensemble mean spatial correlation for a homogeneous image field (Adrian 1988), a perturbation analysis is done for the image field inhomogeneity. The difference with the analysis by Adrian (1988) is that the spatial variation of the ensemble mean intensities is retained. The image fields are interrogated as if they were homogeneous, i.e. the (local) mean image intensity is subtracted. For a practical situation this means that the experimentalist is unaware of the fact that the images are inhomogeneous, and he will use the same method for estimating the particle-image displacement as for homogeneous images. This procedure implies that first the mean image intensity is subtracted from the image fields before computing the spatial correlation.

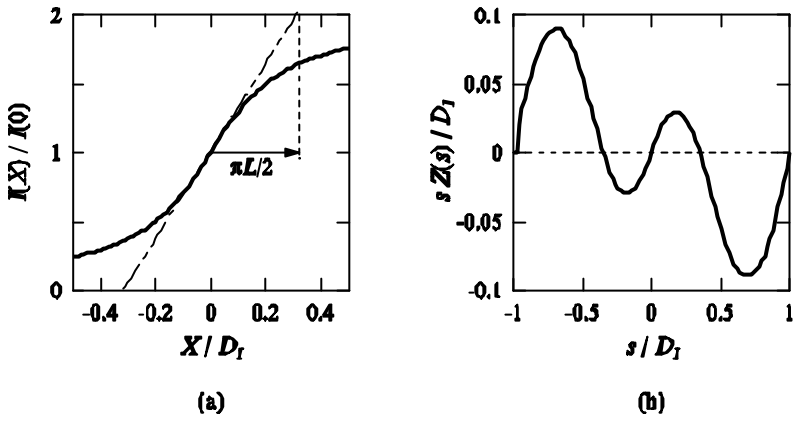

Figure 3 The profiles of: (a) $I(X)$, and: (b) $sZ(s)$, for the expression in (24) with: $L / D_I = 0.2$.

The locally averaged mean image intensities $\bar{I}_1$ and $\bar{I}_2$ are given by:

$$\bar{I}_1 = \frac{1}{D_I^2} \int W_1(\mathbf{X}) \langle I_1(\mathbf{X}) \rangle d\mathbf{X} \quad \text{and} \quad \bar{I}_2 = \frac{1}{D_I^2} \int W_2(\mathbf{X}) \langle I_2(\mathbf{X}) \rangle d\mathbf{X}, \tag{19}$$

respectively. The assumption that the ensemble-mean image intensity is uniform implies an error in the ensemble mean spatial correlation, which can be written as:

$$\langle R(\mathbf{s}) | \mathbf{u} \rangle = \langle R_D(\mathbf{s}) | \mathbf{u} \rangle + \bar{I}_1 \bar{I}_2 D_I^2 Z(\mathbf{s}), \tag{20}$$

where $Z(\mathbf{s})$ is a dimensionless function that represents the inhomogeneity of the image fields, defined as:

$$Z(\mathbf{s}) = \frac{1}{D_I^2} \int W_1(\mathbf{X}) W_2(\mathbf{X}) \frac{\langle I_1(\mathbf{X}) \rangle \langle I_2(\mathbf{X}) \rangle - \bar{I}_1 \bar{I}_2}{\bar{I}_1 \bar{I}_2} d\mathbf{X}. \tag{21}$$

For the denominator in (9) it is assumed that the contribution of $Z(\mathbf{s})$ in (20) is negligible, and for the numerator $Z(\mathbf{s})$ is expanded as a Taylor series around $\mathbf{s} = \mathbf{s}_D$. Substitution in (9) with use of the expressions in (3), (5) and (19) yields the following result:

$$\mathbf{b}(\mathbf{s}_D) \cong \frac{\bar{I}_1 \bar{I}_2 D_I^2 \int \mathbf{s} Z(\mathbf{s}) d\mathbf{s}}{J_1 J_2 t_{00}^2 N_I F_O(\Delta z) F_I(\mathbf{s}_D)} \tag{22}$$

This expression is further evaluated by substitution of $\bar{I}_1 \cong \langle I_1 \rangle = J_1 t_{00} C \Delta z_0 / M_0^2$ (cf. (3) and (19)), and *vice versa* for $\bar{I}_2$, and by a Taylor series expansion of $Z(\mathbf{s})$ around $\mathbf{s} = \mathbf{s}_D$. The integral is taken over a region with an area proportional to d_t^2, i.e. the area covered by the displacement-correlation peak $\langle R_D(\mathbf{s}) | \mathbf{u} \rangle$, which yields the following (approximate) result:

$$\mathbf{b}(\mathbf{s}_D) \cong \mathbf{s}_D N_S \frac{Z(\mathbf{s}_D)}{F_O(\Delta z) F_I(\mathbf{s}_D)}. \tag{23}$$

Note that the bias error vanishes for zero displacement. This is obvious, as any pattern of particle images will perfectly correlate with itself for zero displacement. The bias error is also proportional to the source density,

which essentially reflects that the mean background intensity is directly proportional to the number of particle images in the interrogation region. Hence, the bias error vanishes in the limit of zero source density. This would correspond to the cross-correlation of exactly one particle image (for which the source density is essentially zero, as there can be no overlap with other particle images): there will always be a perfect match of the particle-image pair.

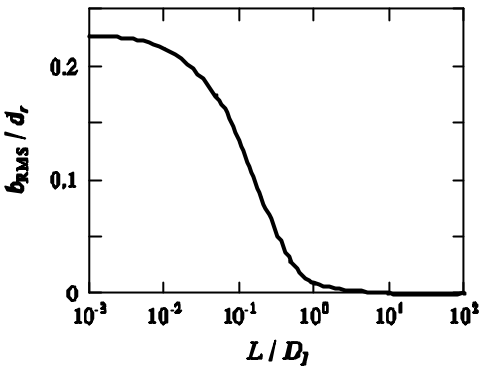

Figure 4 The RMS bias error amplitude (in pixel units) as a function of the length scale L of the light-sheet intensity gradient for a source density $N_S = 0.05$, $D_I / d_r = 32$ and $d_t / d_r = 2$.

4. RESULTS

In this section the analytical result in (23) is evaluated for different situations. In all calculations it is assumed that the out-of-plane motion is negligible, i.e. $F_O \sim 1$. In addition it is assumed that the skewing effect of $F_I(\mathbf{s})$ that was described earlier is accounted for, e.g. by means of normalizing the displacement-correlation peak by F_I, by means of using window matching, or by means of using interrogation windows of different size.

First the effect of light-sheet non-uniformity is investigated. It is assumed that the in-plane intensity distribution of the light sheet is given by:

$$I_1(\mathbf{X}) = I_2(\mathbf{X}) = J \cdot \left[1 + \tfrac{2}{p}\arctan\left(X/L\right)\right], \tag{24}$$

where L is a length scale associated with the gradient of the intensity variation. Substitution of (24) in (21) yields $Z(\mathbf{s})$. The profiles of $I(\mathbf{X})$ and $\mathbf{s}Z(\mathbf{s})$ are plotted in Figure 3 for $L / D_I = 0.2$.

Next the bias error $\mathbf{b}$ is evaluated as a function of L / D_I for $N_S = 0.05$, i.e. $N_I = 16$ and $d_t / D_I = 1/16$. The profile of $\mathbf{s}Z(\mathbf{s})$ in Figure 3b shows that the bias error $\mathbf{b}$ is a function of the displacement. The amplitude of the profile can be characterized by the RMS value taken over the full displacement range $-\tfrac{1}{2} \le s/D_I \le \tfrac{1}{2}$, and this RMS value can be used to evaluate the RMS amplitude $\mathbf{b}_{\mathrm{RMS}}$ of the bias error. In Figure 4 the RMS bias error is plotted as a function of L / D_I. Although the present analysis is carried out for continuous image fields, the bias error is given relative to a pixel dimension d_r that would correspond to a digital interrogation resolution of 32×32 pixels, i.e. $d_r / D_I = 1/32$. The bias error is considered to become significant when it is larger than 0.05-0.1 px, which is the typical random error amplitude for a 32×32-pixel interrogation window with a 2-4 px particle-image diameter (Westerweel 1999). This level of error is also comparable to the bias errors plotted in Figure 2, i.e. -0.003 D_I = -0.10 d_r, for $d_r / D_I = 1/32$. Hence, according to the result in Figure 4, the RMS bias error due to light-sheet non-uniformity becomes significant for L / D_I less than about 0.3. Note that even in the extreme situation that only one half of the interrogation window contains particle images, i.e. $L / D_I \to 0$, the bias error does not exceed 0.25 px. For a light sheet with a Gaussian intensity profile in the case of a 1024×1024-px image and 32×32-px interrogation regions, the maximum gradient of $I(\mathbf{X})$ would correspond to a typical value for L / D_I of about 4. Hence, in any practical situation the intensity profile of a Gaussian light-sheet profile does not lead to a significant bias error in the measured displacement.

Strong gradients in the light-sheet intensity profile would occur in the case of a shadow when a small object is present in the light sheet, e.g. small particles (viz., 'dirt') that are deposited on a window through which the light sheet enters the test section. The intensity profile is now given by:

$$I_1(\mathbf{X}) = I_2(\mathbf{X}) = J \cdot \left[\tfrac{1}{p}\arctan\left(\frac{X - X_S - \frac{1}{2}W_S}{L}\right) + \tfrac{1}{p}\arctan\left(\frac{X - X_S + \frac{1}{2}W_S}{-L}\right)\right] \tag{25}$$

where X_S is the shadow width. In order to represent a shadow with a sharp edge, a value of $L / D_I = 0.001$ is used. The computation and analysis of the RMS bias error is done in a similar way as described above. The profile of $sZ(s)$ for a position of the shadow $X_S / D_I = 0.1$ is plotted in Figure 5b; the result for the RMS bias error as a function of the shadow width X_S / D_I is plotted in Figure 5c. Note that a shadow does not cause a significant bias error for X_S / D_I less than 0.1.

The last situation that is investigated here is that of a gradient in the ensemble mean intensity that moves along with the flow. Such a gradient would be caused by a gradient in the concentration of the tracer particles. The motion of the gradient is equal to the displacement of the particle images, and it is assumed to be described by:

$$I_1(\mathbf{X}) = J \cdot \left[\frac{2}{p}\arctan\left(\frac{X_1 - X_S + \frac{1}{2}s_D}{L}\right)\right], \text{ and: } I_2(\mathbf{X}) = J \cdot \left[\frac{2}{p}\arctan\left(\frac{X_1 - X_S - \frac{1}{2}s_D}{L}\right)\right] \qquad (26)$$

The bias error is evaluated as a function of the position of the gradient for a fixed displacement $s_D / D_I = 0.25$, i.e. the optimal displacement as specified by Keane & Adrian (1990). The result is plotted in Figure 6. The bias error is negative, i.e. it is directed towards the high-intensity region to the left. When the gradient is inverted, i.e. $L / D_I = 0.01$, the bias error becomes positive. For the results presented in Figure 6c the mean bias error is only significant when the 'bright' region occupies less than one half of the interrogation region, i.e. $X_S / D_I < 0$.

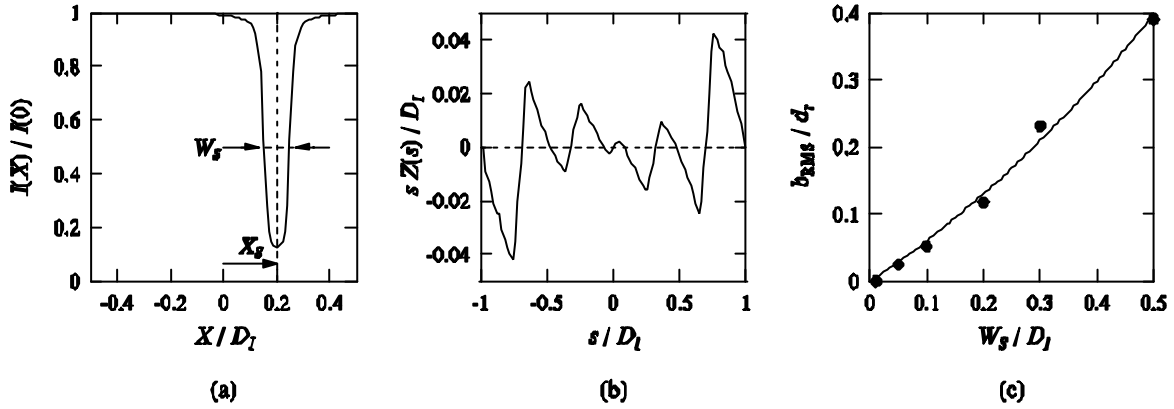

Figure 5 (a) The profile of $I(X)$ for the case of a thin shadow with a width W_S and at a position X_S with respect to the origin of the interrogation region. The intensity gradient in the shadow corresponds to $L / D_I = 0.01$. (b) The corresponding profile of $sZ(s)$ for $W_S / D_I = 0.1$ and $X_S / D_I = 0.2$. (c) The RMS bias error as a function of the shadow width W_S / D_I for $N_S = 0.05$, $D_I / d_r = 32$ and $d_t / d_r = 2$.

5. CONCLUSIONS

An expression is derived that describes the effect of image inhomogeneity on the ensemble-mean of the measured displacement. In general, inhomogeneity of the image intensity field leads to bias errors in the measured displacement field. Three different situations are evaluated: (1) a gradient in the light-sheet intensity profile; (2) a thin 'shadow' in the interrogation region; and (3) a gradient in the particle-image intensity that moves along with the tracer pattern. In all cases the bias errors are very small, i.e. of the order of the particle-image diameter, but for certain situations the bias error becomes significant with respect to the amplitude of the random error.

The analysis results imply that the correlation analysis of the interrogations regions is quite robust with respect to variations in the image intensity, although significant errors on the level of the random error amplitude may occur. One should bare in mind that the present analysis was carried out for a uniform displacement field, and that in a practical situation a spatial variation in the image statistics is usually coincides with a spatial gradient in the velocity field (e.g., a shock wave or the boundary of a jet). Since the variation of the (ensemble) mean image properties do not contribute significantly to the bias error, it is conjectured that in this situation the shape of the displacement-correlation peak is given by the weighted mean of the displacement over the interrogation domain, where the relative weight is given by the (ensemble) mean intensity.

In order to validate the present analytical result it would be necessary to perform a series of simulations by means of generating synthetic PIV images that have the same properties as the image fields that were investigated analytically. Such simulations are currently under consideration.

REFERENCES

Adrian, R.J. (1988) "Statistical properties of particle image velocimetry measurements in turbulent flow." In: *Laser Anemometry in Fluid Mechanics — III*} (Eds. R.J. Adrian *et al.*) LADOAN Instituto Superior Tecnico (Lisbon) 1988, pp. 115-129.

Keane, R.D. & Adrian, R.J. (1990) "Optimization of particle image velocimeters. Part I: double pulsed systems." *Meas. Sci. Technol.* **1,** 1202-1215.

Keane, R.D. & Adrian, R.J. (1992) "Theory of cross-correlation analysis of PIV images." *Appl. Sci. Res.* **49**, 191-215.

Prasad, A.K., Adrian, R.J., Landreth, C.C. & Offutt, P.W. (1992) "Effect of resolution on the speed and accuracy of particle image velocimetry interrogation." *Exp. Fluids* **13**, 105-116.

Westerweel, J. (1997) "Fundamentals of digital particle image velocimetry." *Meas. Sci. Technol.* **8**, 1379-1392.

Westerweel, J. (1998) "Effect of sensor geometry on the performance of PIV interrogation." In: *Developments in Laser Techniques and Fluid Mechanics* (Eds. R.J. Adrian *et al.*), Springer-Verlag, Berlin.

Westerweel, J. (1999) "Theoretical analysis of the measurement precision in PIV." In: *Proc. 3rd Int. Workshop on PIV* (Santa Barbara, CA), Sept. 16-18, 1999.

Willert, C.E. & Gharib, M. (1991) "Digital particle image velocimetry." *Exp. Fluids* **10**, 181-193.

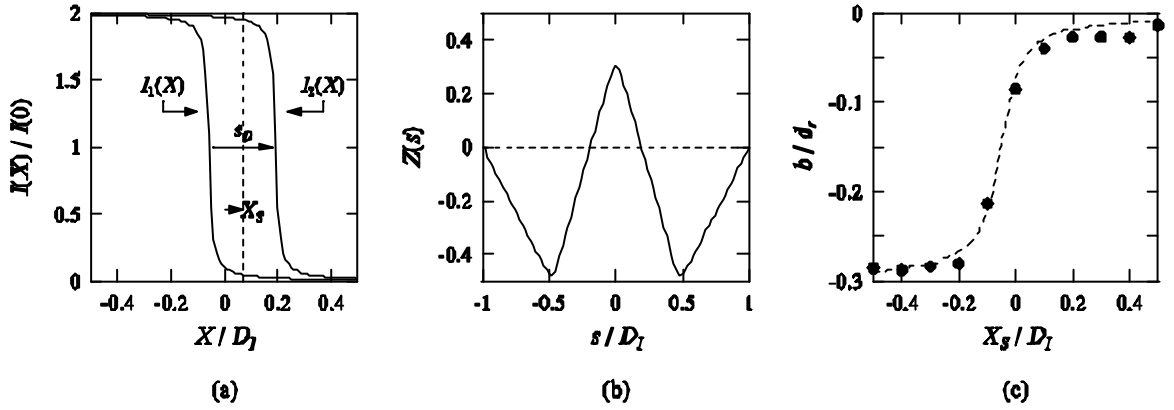

Figure 6 (a) The profiles of $I_1(X)$ and $I_2(X)$ defined in (26) for $L / D_I = -0.01$. (b) The corresponding profile for $Z(s)$ with $X_S / D_I = 0.1$ and $s_D / D_I = 0.25$. (c) The bias error b (in pixel units) as a function of X_S / D_I for $s_D / D_I = 0.25$, $N_S = 0.05$, $D_I / d_r = 32$ and $d_t / d_r = 2$. (The dashed line is only intended to guide the eye.)